Chapter 2

Supramolecular Organization of Amyloid Fibrils

Dmitry Kurouski

Additional information is available at the end of the chapter

http://dx.doi.org/10.5772/62672

Abstract

The current chapter illustrates how both electron and scanning probe microscopy can be utilized to unravel the supramolecular organization of amyloid fibrils, β-sheet-rich protein aggregates, which are strongly associated with various neurodegenerative diseases. It also discusses why morphologically different fibrils can be grown from the same protein under slightly different experimental conditions, which is a phenomenon known as fibril polymorphism. Next, it establishes the high potential of vibrational circular dichroism (VCD) for unraveling the supramolecular organization of amyloid fibrils. Finally, it discusses several hypotheses of amyloid fibril formation that were developed based on numerous microscopic and spectroscopic studies.

Keywords: amyloid fibrils, supramolecular chirality, microscopy, VCD, polymorphism or fibril polymorphism

1. Introduction

Under normal physiological conditions, the native structure of partially unfolded proteins is restored by numerous self-sustaining pathways of cell homeostasis. However, under some pathological conditions, such as neurodegenerative diseases, partially unfolded proteins may adopt β-sheet structure [1, 2]. This primarily happens because the β-sheet structure is energetically more favorable when compared to the native structure of the protein. When two β-sheet moieties associate together plane-to-plane, they form a very stable structure, known as a cross-β-sheet. The cross-β-sheet is capable of templating the aggregation of misfolded or partially unfolded proteins. As a result, fibril filament, the simplest supramolecular architecture, is formed. It stretches microns in length in the direction perpendicular the peptide strands in the β-sheets [3–5]. Following electrostatic energy minimization, filaments tend to twist along their longitudinal axis. And as a result, local charges on the fibril surface increase their mutual distance.

Contrastingly, twisted filaments have much higher elastic energy than a flat structure. And consequently, the filaments tend to adopt becoming as relaxed and flat geometrically as possible to reach the elastic energy minimum. The net between these two competing energies, electrostatic and elastic, determines the degree of the filament twist [6, 7].

Twisted filaments also braid and coil with other filaments [8–10], forming higher hierarchical supramolecular structures named proto-fibrils and fibrils [11, 12]. Alternatively, twisted filaments may associate side-by-side, forming cross-β-sheet tape-like fibrils [10, 11]. Different filaments' propagation pathways result in a large diversity of fibril morphologies. This phenomenon is known as fibril polymorphism [3, 13]. *Post-mortem* microscopic examination of fibrils that were detected in the organs and tissue of patients, who were diagnosed with different neurodegenerative diseases, also revealed their morphological heterogeneity [14, 15]. Moreover, *in vitro* studies have demonstrated that morphologically or structurally different fibril polymorphs had different toxicity [16]. And as a result, a clear understanding of fibril supramolecular organization will help to unravel the origin of fibril toxicity.

Methodologically, unraveling the supramolecular organization of amyloid fibrils is a challenging task. This is primarily because fibrils are insoluble and cannot be crystalized, which unfortunately limits X-ray and NMR, classical tools of structural biology, for their studies [17, 18]. Historically, microscopy was the first, and most commonly utilized technique which is capable of unraveling supramolecular organization of amyloid fibrils. There are several microscopes that are effective in resolving amyloid aggregates which include: electron (EM), transmission (TEM), and scanning electron (SEM) microscopes, and lastly probe microscopes. In addition to microscopy, vibrational circular dichroism (VCD) can directly probe supramolecular organization of amyloid fibrils [11, 19]. It was recently discovered that VCD can detect the twist of the fibril filaments, which not always may be visualized using SEM or atomic force microscopy (AFM) [8]. The observed VCD intensities of fully developed fibrils and their filaments are one to two orders of magnitude larger than VCD intensities observed from solutions of individual proteins. This indicates that enhanced VCD arises from the long-range supramolecular chirality of fibrils, making VCD a unique *solution-phase*, stereospecific probe of protein fibril structure and chiral morphology. A growing body of literature indicates that VCD has already become a powerful and broadly used tool for the supramolecular characterization of amyloid aggregates [11, 20, 21].

2. Unraveling supramolecular chirality of amyloid fibrils using microscopy

Conventional light microscopy is not capable of visualizing individual amyloid aggregates due to their small sizes. According to Abbe diffraction limit, a resolution (d) directly depends on a wavelength of light (λ), where α is the half-angle of the maximum cone of light that can enter the microscope objective (1).

$$d = \frac{\lambda}{2\sin(\alpha)} \quad (1)$$

For a microscope objective, the aperture angle is described by the numerical aperture (NA), where NA = n•sinα (n is a media refractive index). Consequently, *d* of any confocal microscope can be expressed as (2).

$$d = \frac{0.61\lambda}{NA} \quad (2)$$

The expression 2 indicates that the resolution increase with the decrease in the wavelength and an increase in the NA of the objective. The best optical systems would be equipped with 100× oil immersed objective (NA=1.4) will give the resolution of ~200 nm. At the same time, amyloid fibrils, as we will discuss below, are only 10–20 nm in diameter. Nevertheless, it should be mentioned that the light microscopy is the most commonly utilized technique in the clinical practice for the confirmatory diagnostic of amyloid plaques. Upon staining with Congo-red, in the linearly polarized light, these amyloid deposits exhibit green birefringence.

Recently invented super-resolution microscopy, such as photoactivated localization microscopy (PALM) and direct stochastical optical reconstruction microscopy (d-STORM), allowed for overcoming the Abbe diffraction limit and reach 2–10 nm spatial resolution [22–24]. For example, d-STORM was capable of resolving individual amyloid β aggregates [25]. However, very limited information about their supramolecular organization could be obtained. Partially, because sample labeling with fluorophores is required, which obscures tiny details of fibril topology. Also, since there are only a few fluorophores are activated per every light exposure in super-resolution microscopy, long acquisition time is typically required for an image processing. Therefore, thermal drift of current super-resolution microscopes becomes the serious issue which limits their spatial resolution.

2.1. Unraveling the shape and localization of amyloid fibrils by TEM

The invention of the electron microscope, by Max Knoll and Ernst Ruska at the Berlin Technische Hochschule, in 1931, allowed for overcoming the limitation of a visible light in obtaining higher spatial resolution. Using TEM, the first morphological characterization of the individual amyloid fibrils was achieved [26, 30]. This microscopic technique is relatively facile when compared to other microscopic tools which will be discussed below. In most cases, only a drop of the analyzed sample is needed to be placed onto a carbon or formvar-coated Cu film support and dried under ambient conditions. Uranium or osmium salts are often applied to the dried sample to increase the contrast of biological samples. Alternatively, samples for TEM can be prepared by cutting plastic embedded biological samples. For example, TEM imaging of the thin-cut plastic embedded amyloid tissues revealed long unbranched rod-like aggregates that were named amyloid fibrils (**Figure 1A**) [26–29]. Aggregates with the same morphology were

later reported by M. Kidd upon TEM imaging of the extract of amyloid-loaded liver tissue (**Figure 1B**) [30].

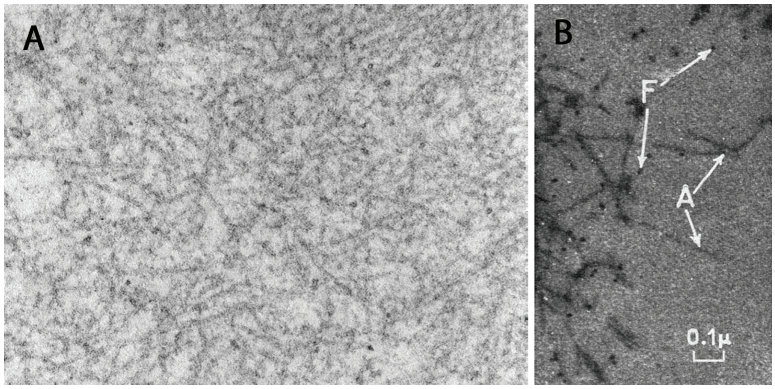

Figure 1. TEM images of amyloid fibrils in (A) thin-cut plastic embedded amyloid tissue (×50,000) and (B) extract of amyloid-loaded liver tissue. Locations of amyloid fibrils and their twisted filaments are marked by "A" and "F" respectively. Adapted from Tosoni et al. [26] and Kidd [30].

Aggregates of Tau proteins, histologically known as neurofibrillary tangles, are commonly co-present together with amyloid plaques in brains of patients, who have been diagnosed with Alzheimer's disease. Their detailed microscopic study conducted by Wischik et al. (**Figure 2**) [14, 15]. Using TEM, Wischik et al. studied the extracts from the human brains that contained neurofibrillary tangles. Authors observed fibrils with flat and twisted topologies. Using metal

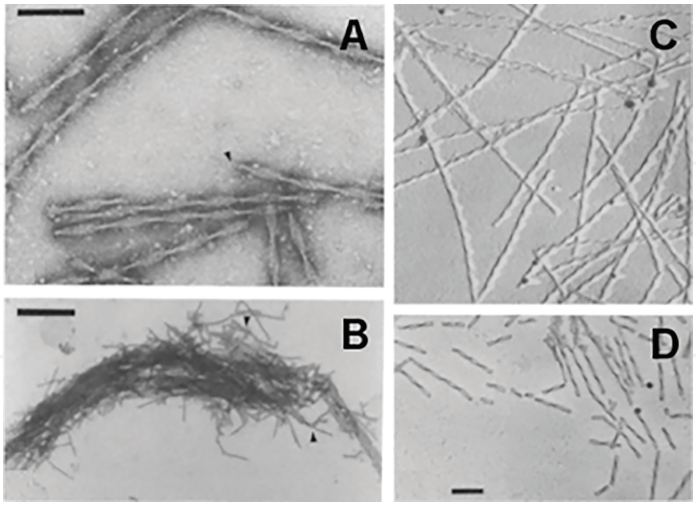

Figure 2. TEM images of uncoated (A, B) and metal coated (C, D) Tau fibrils extracted from the human brain. Scale bards are 100 nm (A, C, D) and 1000 nm (B) [14, 15].

http://dx.doi.org/10.5772/62672

shadowing, Wischik et al. determined the twist direction, which appeared to be left-handed. Additional, it was discovered that these left-twisted fibrils were composed of two intertwined left-handed proto-fibrils. The exposure of left-twisted fibrils to an alkali solution led to their untwining, which made Wischik et al. to conclude that the integrity of left-twisted fibrils was held by electrostatic interactions between their proto-fibrils.

These pioneering works were followed by numerous studies that report TEM microphotographs of various protein aggregates and amyloid fibrils [31, 32]. It has been demonstrated that TEM was capable of detecting twists in ribbon-like fibrils, curvature of fibrils, and the roughness of their surfaces. TEM images could also be used to obtain quantitative data, including dimensions of fibrils and their precursors, such as oligomers and filaments. In addition, TEM was able to reveal a number of filaments in the mature fibril, as well as the periodicity of the fibril twists. However, in most cases, TEM imaging was simply used to confirm a presence of fibril species rather than to provide their morphological characterization. This is in parts because such microscopic examination can be performed relatively quickly, allowing researchers to verify whether fibril formation has occurred or not.

In parallel, TEM was used to monitor changes in the structure of mature fibrils which were caused by various chemical and physical factors [33, 34]. For example, it has been demonstrated that integrity of insulin fibrils could be perturbed through alteration of fibril electrostatic interactions [33]. Shammas et al. exposed insulin fibrils which were grown at pH 2 to solutions with pH 4, 6, 8, 10, and 12. Using TEM, Shammas et al. found that at pH above 4 insulin fibrils drastically changed their morphology (**Figure 3**). Moreover, full disintegration of fibrils was observed if the solution pH was higher than pH 10. It has been concluded that these changes were caused by the strong electrostatic repulsion of the protein amino acid sequence in the fibril cross-β-sheet.

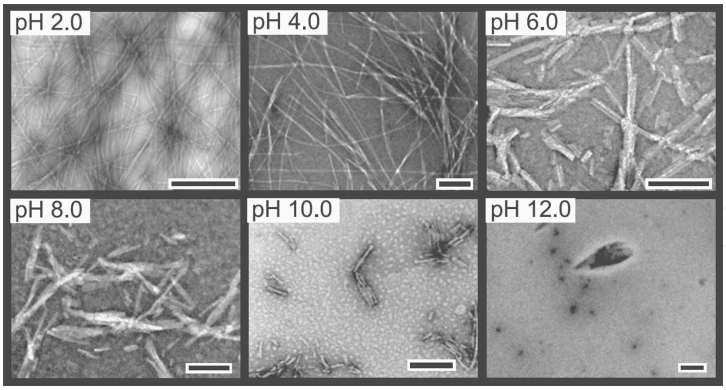

Figure 3. TEM images of insulin fibrils (pH 2.0) after prolong exposition in solvents with higher pHs. Scale bars are 200 nm [34].

Separately, using VCD, Kurouski et al. demonstrated that a small change in pH drastically changes morphology and supramolecular chirality of insulin fibrils [35]. This process was

irreversible and occurred only when the pH was raised from 1.5 to 2.5. No effect of solution ionic strength was found. An addition of sodium chloride up to 1 M concentration to pH 1.5 fibrils did not change the kinetics of the polymorphs' inter-conversion.

2.2. Mass-per-length measurements of amyloid fibrils using scanning transmission electron microscopy

As the analog of TEM, scanning transmission electron microscopy (STEM) is often used to explore the morphological organization of amyloid aggregates. Similar to TEM, the background of STEM images has lower intensity than protein specimens. This is due to stronger electron scattering from protein aggregates comparing to a thin carbon film on which they are adsorbed on. As a result, STEM image intensities appear to be proportional to mass densities (per unit area). This can be used to determine mass-per-length (MPL) values of the analyzed specimens [17, 36, 37]. MPL can be determined directly by measuring the incident electron beam flux if the electron scattering cross-sections, as well as the detector geometry and sensitivity are known. Alternatively, MPL can be evaluated by a comparison of the intensities of the analyzed specimens with the intensities of objects with known mass densities. Tobacco mosaic virus (TMV) is the most commonly used reference for such a comparison-based MPL imaging. MPL values can be utilized to determine secondary structure of amyloid fibrils. For

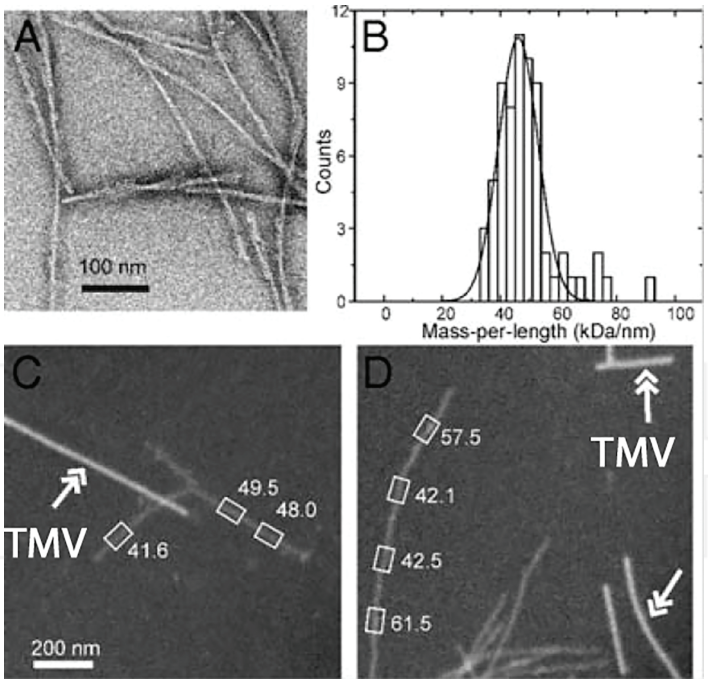

Figure 4. TEM microphotograph (A) of amyloid fibrils grown from Rnq1 prion and their MPL (B) histogram. STEM microphotographs (C and D) or the same fibrils and TMV rods (indicated by double-headed arrows). MPL values (kDa/nm) are shown for fibril segments enclosed in rectangles [39].

example, using MPL, it has been found that 40-residue amyloid β peptide (Aβ1–40) formed two distinct fibril polymorphs with 2- and 3-fold symmetry [36]. MPL measurements confirmed a β-helix-like structure of HET-s prion (HET-s218–289) protein fibrils, where each peptide molecule spanned two turns of the β-helix [38]. It has been also shown that MPL measurements could be used to investigate structural organization of fibrils formed by the yeast prion protein Rnq1 (**Figure 4**) [39]. Chen et al. found that the prion sequence was folded into in-register parallel β-sheet structure, with one Rnq1 molecule per 0.47-nm β-sheet repeat spacing.

2.3. Probing topology and supramolecular chirality of amyloids by SEM

In SEM, both detector and the electron source are located on the same side of the sample. Consequently, only scattered electrons (rather than electrons that go through the sample, as in the case of TEM) are used to obtain the image of the analyzed specimen. SEM also requires much lower energy of the electron beam (0.2–40 keV vs 100–120 keV, as used for TEM) to obtain the contrast image. Similar to TEM, protein samples, such as amyloid fibrils, are commonly stained with uranium or osmium salts prior to microscopic examination to gain a better contrast. While SEM is not capable of resolving amyloid fibrils in the fixed tissues, it provides excessive morphological information about the *in vitro* prepared or *ex vivo* extracted fibrils. One of the most valuable sides of SEM morphological examination is its capacity to determine the twist handedness of amyloid fibrils. For example, using SEM Rubin et al. evaluated supramolecular chirality of fibrils grown from short amino acid fragments of serum amyloid A (SAA) protein [40, 41]. SAA are a group of apolipoproteins associated with high-density

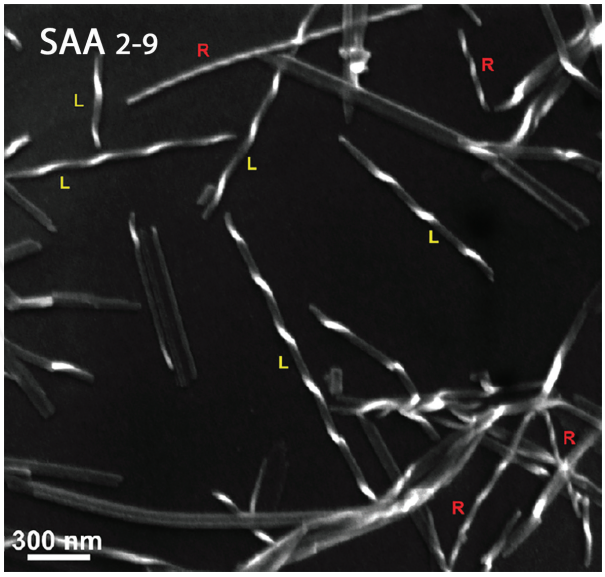

Figure 5. SEM image of simultaneously grown amyloid fibrils of serum amyloid A SAA_{2-6} peptide that exhibit left- and right-twisted fibrils [40].

lipoprotein (HDL) in blood plasma that are often expressed in response to inflammatory stimuli in liver.

Rubin et al. found that SAA fragment with the sequence SFFSFLG ($SAA_{2–6}$) simultaneously formed both left- and right-twisted fibrils (**Figure 5**). It was also found that fibrils with the same twist direction had different twist periodicity. Some of the right-twisted fibrils were highly twisted (**Figure 3**, fibril marked R at the top), while others had much more of a loose twist (**Figure 3**, fibrils marked R on the right and bottom). This indicated that several right-twisted fibril polymorphs have simultaneously grown. Rubin et al. also discovered that $SAA_{2–12}$ with the sequence SFFSFLGEAFD exclusively formed right-twisted fibrils, while its analog with only two different amino acids, $SAA_{1–11}$RSFFSFLGEAF aggregated in 100% left-twisted fibrils [40]. This discovery suggested that amino acid sequence may control the supramolecular chirality of amyloid aggregates.

At the same time, Kurouski et al. demonstrated that fibril morphology and supramolecular chirality can be directly controlled by pH [8, 42]. Insulin and lysozyme aggregation at pH below 2 (25°C) led to a formation of tape-like flat fibrils [11]. At the same time, at pH above this point, both of these proteins formed left-twisted fibrils (**Figure 6**) [8]. A fragment of transthyretin (105–115) and HET-s prion (HET-s218–289) protein, on the opposite, formed left twisted fibrils at low pH (25°C), while their aggregation at pH above 2.5 resulted in flat tape-like fibrils [11]. HET-s is a prion protein of the fungus *Podospora anserine*, which C-terminus fragment is capable of forming amyloid fibrils at low pH. Authors suggested that protonation/deprotonation of aspartic and glutamic amino acid residues, as well as peptide C-termini, which was taking place around this pH, changed the charge on the surface of the filaments. As a result, filaments adopted either left-handed or right handed twist. Left twisted filaments tended to braid and coil forming left-handed fibrils. At the same time, right twisted filaments associated side-by-side forming tape-like fibrils [11].

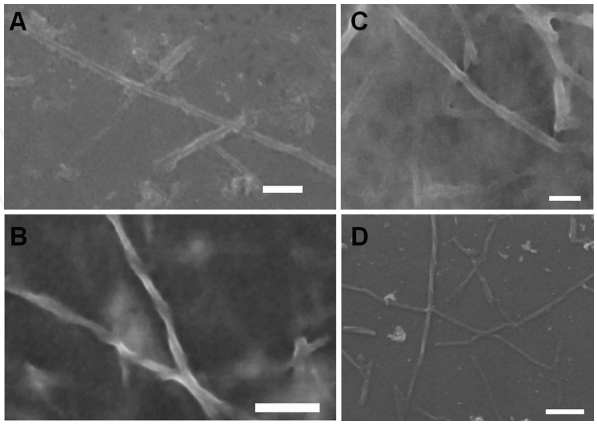

Figure 6. SEM images of insulin (A, B) and lysozyme (C and D) tape-like (top panel) and twisted (bottom panel) fibrils [8]. Twists on the fibril surface are marked by red arrows. Scale bars are 100 nm.

http://dx.doi.org/10.5772/62672

2.4. Application of cryo-SEM for determination of amyloid fibril topology

Typically, both TEM and SEM require sample dehydration. Protein specimens in general and amyloid fibrils in particular are very sensitive to dehydration, which may cause drastic changes in their morphology. To overcome this limitation, cryo-procedure of the sample preparation is often used. In cryo-SEM, protein specimens are imaged at temperature below ambient (typically between −100 and −175°C). This allows for the sample to be preserved and recorded in the fully hydrated and chemically unmodified state.

Cryo-SEM has been extensively used to investigate supramolecular organization of amyloid aggregates that strongly associated with Alzheimer's and Parkinson's diseases. For example, using cryo-EM, Meinhardt et al. found that Aβ(1–40) peptide could form amyloid fibrils with a range of different morphologies [43]. Authors showed that proto-fibrils could associate either side-by-side, forming tape-like fibrils, or coil (intertwine), forming twisted cables. It has been also shown that despite the width of the coiled fibrils varied from 10 to 21 nm, all of them exhibited the same left-handed twist with a turnover from 65 to 163 nm. It was concluded that such difference in the fibril thickness could be due to a different number of proto-filaments that were taking place in their formation [44].

Antzutkin et al. investigated an aggregation of Arctic mutant of Aβ(1–40). It has been shown that this peptide formed seven fibril polymorphs (three non-coiled and four coiled) if aggregated at pH 7.4, 22°C [45]. Moreover, Antzutkin et al. demonstrated that these fibril polymorphs with different morphologies had dramatically different growth rates. It has been found that Aβ(1–40) fibril morphologies could have significant variations in both width and twist tightness, depending on the ionic strength (and the nature of ions) in the aggregation solution [46]. Finally, Petkova et al. investigated the sample agitation impact on the morphology of Aβ(1–40) fibrils. Using microscopy and solid-state NMR (ss-NMR), significant structural differences between fibrils that were grown with and without agitation were found [47].

Supramolecular organization and polymorphism of Aβ(1–42) fibrils are much less investigated comparing to Aβ(1–40) fibrils. Using cryo-SEM, Lührs et al. investigated structural organization of Aβ(1–42) fibrils and found that they were composed of several filaments that had ~2.5 nm in height and around 4.5 nm in width [48]. These filaments braided and coiled together forming thick left-handed cables. Later, Zhang et al. confirmed that Aβ(1–42) formed exclusively left-handed fibrils [49]. It has been also suggested that Aβ(1–42) filaments intertwined around each other, forming a hollow core.

In 2008, Vilar et al. reported results of a very detailed investigation of supramolecular organization of α-synuclein fibrils [50]. Using cryo-SEM and ss-NMR, Vilar et al. found that α-synuclein aggregated formed straight filaments that were around 2 nm in width. These filaments tended to dimerize into thicker proto-fibrils via side-to-side association, forming straight tape-like fibrils. At the same time, they it has been noticed that these filaments could braid together forming left-handed proto-fibrils, with a diameter of ~6.5 nm, and fibrils with a diameter of 9.8 nm (**Figure 7**) [50]. In fact, both straight and twisted α-synuclein fibril polymorphs were detected upon the *post mortem* examination of brains of people who were diagnosed with Parkinson's disease [51, 52].

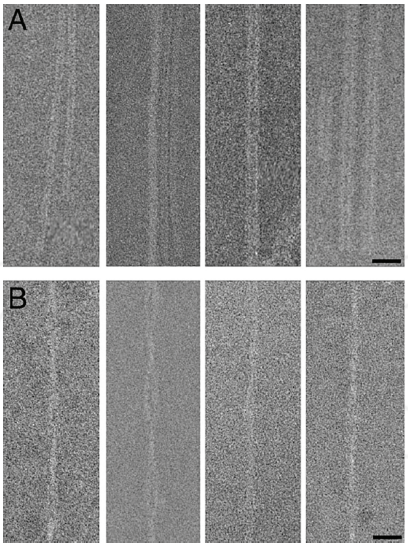

Figure 7. Cryo-SEM images of tape-like (top row) and twisted (bottom row) α-synuclein fibrils. Scale bars are 20 nm [50].

Recently, using cryo-SEM, Rubin et al. examined how the absolute chiral configuration of the amino acids in a peptide sequence impacts on the supramolecular organization of the peptide aggregates [41].

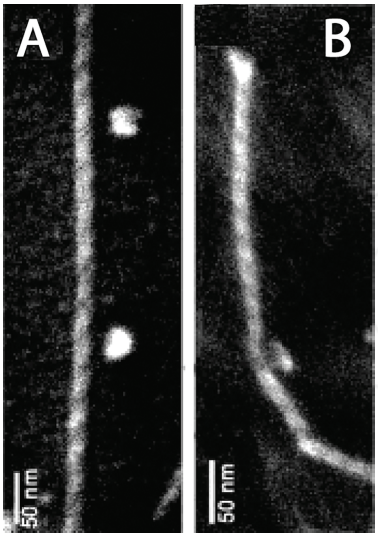

Figure 8. Cryo-SEM images of fibrils grown from all-L amino acid (A) and all-R (B) amino acid fragment of serum amyloid A (SAA_{1-12}) protein [41].

http://dx.doi.org/10.5772/62672

It has been found that all L amino acid peptide with the sequence RSFFSFLGEAFD ($SAA_{1–12}$) formed right-handed fibrils (**Figure 8**). At the same time, aggregation of the same amino acid sequence with all D amino acids led to a formation of exclusively left-twisted fibrils. Separately, Harper et al. demonstrated the same for $A\beta_{(1–40)}$ peptide. It has been found that all L amino acid $A\beta_{(1–40)}$ peptide formed left-handed fibrils twist. At the same time, aggregation of all D amino acid peptide $A\beta_{(1–40)}$ resulted in right-handed fibrils. These experimental pieces of evidence demonstrate that absolute chiral configuration of the peptide sequence may determine whether one or another chiral polymorph will be grown.

2.5. AFM is capable of unraveling mechanisms of fibril formation and structural organization of amyloids

In AFM, silicon or silicon nitride cantilever is used to image the sample. Changes in the frequency of tip oscillation, as it is moved across the surface (tapping mode AFM), are recorded by the laser that is reflected from the back side of the cantilever. As higher the object on the surface, as smaller becomes the amplitude of the tip oscillation. In another modification of AFM, known as contact-mode AFM (CM-AFM), the tip is not oscillating above the surface, but rather steadily kept at it. When CM-AFM tip is moved across the surface, it simply reflects its roughness, similar to a finger of a blind person who reads the Braille font. One can imagine that the CM-AFM cantilever can easily damage fine protein samples upon such microscopic examination. This much rarely happens in AC-AFM because the tip is being repulsed from the surface as soon as van der Waals forces appear between the two. Therefore, CM-AFM is much less frequently used for imaging biological samples, including amyloid fibrils.

One advantage of AFM over EM is its ability to image the specimen without any dehydration or fixation. This is extremely important for microscopic characterization of protein samples, such as amyloid fibrils. It should be noted that AFM provides an accurate height of the imaged specimen, while width often appear slightly larger than the real width of the imaged object. This error is known as the tip convolution effect. It arises from the tip that is used for the sample imaging: as larger the tip diameter and smaller the object on the surface, as larger the tip convolution error. Therefore, AFM and SEM are commonly used complimentary to each other for a determination of accurate height (AFM) and width (SEM) of the analyzed specimens [8, 11].

Using AFM, Mezenga group recently investigated aggregation of bovine serum albumin (BSA) [53]. Usov et al. found that BSA aggregated forming flexible filaments with left-handed twisted morphology. On later stages of fibril formation, they observed rigid fibrils that either had no twist or were right-twisted. Usov et al. proposed that tube-like structures could be formed if the left-twisted filaments would continue twisting along their longitudinal axis. Such super-twisting would finally result in a formation of a hollow tube. Usov et al. also proposed that observed right-handed twisted ribbons could be formed if left-handed filaments would continue to twist passing through the tube stage. This paradigm is very easy to visualize with a piece of rope. If a degree of left-handed twist will be increased, the left-twitted rope would suddenly start making right-handed twists. Therefore, Usov et al. concluded that observed right-twisted fibrils had the left-handed twist of their internal filaments [53].

Adamcik et al. recently demonstrated that the degree of the fibril twist could be changed by the solvent ionic strength. It has been shown that if β-lactoglobulin was aggregated in 100 mM NaCl, it formed tape-like fibrils. However, at 0 mM NaCl, grown fibrils tended to adopt a left-handed twist. It has been concluded that as lower the ionic strength, as higher the twist degree of the formed β-lactoglobulin fibrils [54].

Mezzenga group also explored how pH controlled supramolecular organization of amyloid fibril growth at water-air interface (AWI) [55, 56]. It was discovered that small change in pH caused significant differences in interfacial properties of β-lactoglobulin fibrils, such as their alignment, entanglement, multilayer formation, and fibril fracture. For example, at pH 2, β-lactoglobulin fibrils did not change their aggregation state after 5-hour exposition at AWI (**Figure 9**). However, at pH 3, these fibrils tended to associate into bundles rather than stay in nematic domains. It has been concluded that such drastic changes were caused by the change of the charge on the fibril surface [56].

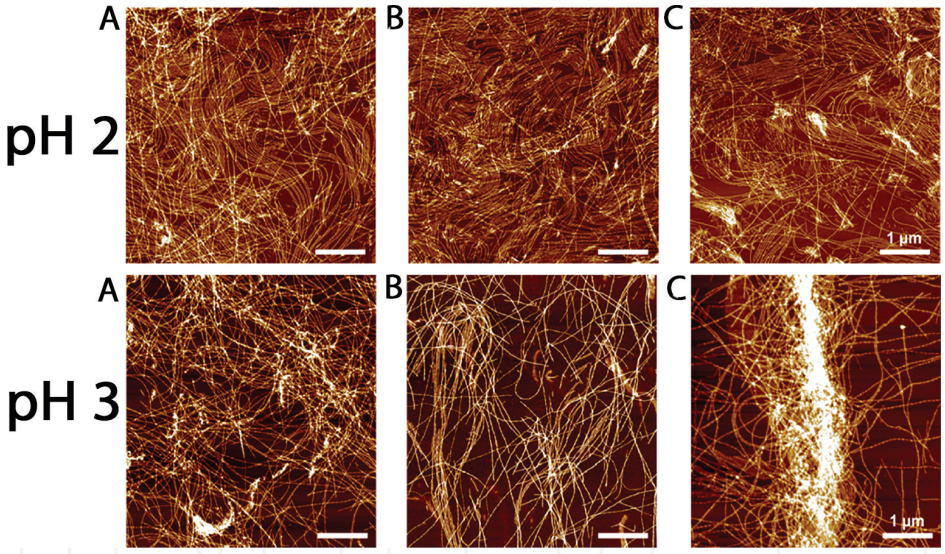

Figure 9. β-Lactoglobulin fibrils on water-air interface at pH 2 (top) and 3 (bottom) after (A) 1, (B) 2, and 5 hours (C). Modified from Jordens et al. [56].

Nearly a decade ago, it was demonstrated that vortexing of insulin solutions during protein aggregation at 60°C caused formation of similar bundled fibril superstructures [57, 58]. In addition to AFM, Dzwolak group explored chiroptical properties of these insulin bundles using induced circular dichroism (ICD) [59]. In ICD, an achiral chromophore is used to probe the structure of a chiral molecule that has very low intensity of circular dichroism signal. It has been found that these fibril superstructures are capable of binding thioflavin T (ThT), which results in a negative induced circular dichroism (−ICD). However, if the protein aggregation

was carried out at steady-state conditions, insulin fibrils did not form bundles and consequently no enhanced ICD signal was observed.

Mezzenga group also explored aggregation of α-synuclein at AWI and solid-liquid interfaces using AFM [60]. They found that at AWI, α-synuclein rapidly aggregated into amyloid fibrils that remained adsorbed to the AWI. Instead, when the protein aggregation was taken place at solid-liquid interface, α-synuclein aggregation is greatly reduced. This finding demonstrated that protein aggregation is a very complex process that can be altered by varying solution conditions and presence of interfaces that can either accelerate or decelerate fibril formation.

Separately, Qin et al. aggregated α-synuclein in similar conditions (10 mM phosphate buffer, pH 7.4) and found that mature fibrils have a left-handed twist [61]. They also elucidated the role of two terminal fragments of α-synuclein. It was found that the protein without the first 29 amino acids from the N terminus (syn30–140) formed fibrils similar to the intact α-synuclein. These fibrils had a right-twisted twist and were composed of two filaments and were around 107 nm in height (AFM), **Figure 10**.

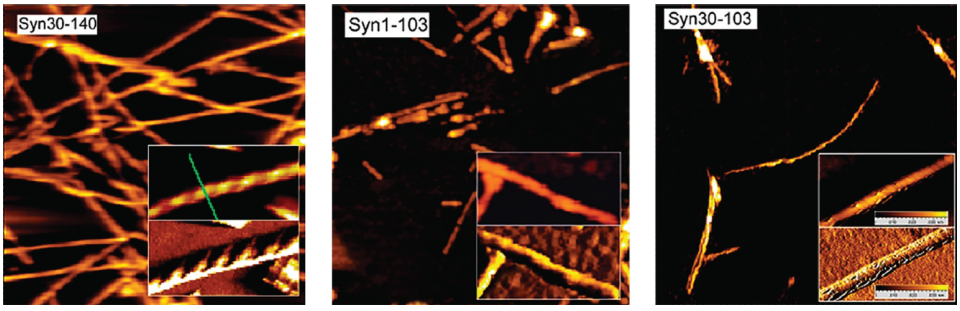

Figure 10. Morphology of the fibrils derived from three truncated α-synucleins. The inserted panels in each AFM image are a single fibril (upper) and its second derivative image (lower). Syn30–140 fibrils show long, straight morphology, and the double-filament twisted structure is observed in the enlarged fibril and its second derivative images (attributed to a pair of twisted protofibrils). Syn1–103 gives much thinner fibrils, but double-filament twisted structure is also observed (attributed to a protofibril consisting of two protofilaments). Syn30–103, however, shows very thin fibrils with a single filament and untwisted structure (attributed to a protofilament) [61].

Intriguingly, according to their AFM images, full-length α-synuclein fibrils were almost 140 nm in height. It has also been found that C-terminal truncated α-synuclein (syn1–103) was able to aggregate. However, this 103 amino acid peptide formed fibrils with smaller height (~57 nm). These fibrils, like syn30–140, also exhibited a right-handed twist. According to the Qin et al., syn1–103 fibrils looked rather like proto-fibrils than mature fibrils [61]. Based on this observation, authors made a conclusion that C-terminus of α-synuclein was highly important for the assembly of two proto-fibrils into a mature fibril. Finally, the central sequence fragment of α-synuclein that lacked both N- and C-termini, syn30–103, was found to be able to aggregate forming long un-branched fibrils. However, these fibrils were only 28.8 nm in height with no clear twist evident from the obtained AFM images.

Using AFM, Jansen et al. performed a detailed investigation of insulin aggregates that were grown at pH 1.6 [62]. It was determined that insulin proto-fibrils, which had around 1.2 nm in diameter, intertwined, forming left-handed fibrils with 3–7 nm in diameter. In addition, right-handed fibrils were simultaneously observed. Intriguingly, that it has been proposed that these right-handed fibrils were formed not as a result of proto-fibril coiling, but rather as a result of a lateral aggregation or small fibril blocks (10 × 60 nm). This aggregation mechanism will be further discussed in the last section of this chapter. This type (side-by-side) of aggregation was also proposed as the origin of binary, tape-like ribbons that were also observed upon insulin aggregation. Finally, authors observed that many insulin fibrils formed from small (~150 nm in length) subunits that are linearly extend one other. Based on this observation, Jansen et al. proposed that insulin fibrils can assemble via chainlike quenching of these subunits.

Human amylin is a 3.9 kDa protein secreted by islet β-cells of the pancreas. Together with insulin, it is involved in glucose metabolism. Amylin fibril aggregates are toxic and strongly associated with diabetes type II. Upon *invitro* aggregation at neutral pH (7.4), amylin forms thin proto-fibrils, which are around 5 nm in width and tend to aggregate further, forming two morphologically distinct polymorphs. In one case, proto-fibrils intertwine (coil), and form cable-like structures 8–10 nm in width with a distinct left-handed twist with a crossover of 25 nm. These cable-like structures could coil further, forming thick left-handed cables with larger widths. In addition, the height of these twisted fibrils has been determined. It has been shown that it varies from 3 (proto-fibrils) to 7 nm mature fibril cables [63]. Alternatively, three, four, or more proto-fibrils could aggregate side-by-side, forming flat, single-layer ribbons. Intriguing that the ribbons also twist at moderate regular intervals in a left-handed fashion [31]. Based on these observations, Goldsbury et al. proposed that amylin fibril polymorphism originated from different ways of proto-fibril associations, while all observed fibril polymorphs have the same structure [64]. There was no clear understanding about the nature of a force that determined the formation of either type of those polymorphs. Three years later, Goldsbury et al. investigated aggregation of the full-length amylin (37 amino acids) and two fragments of amylin: 8–37 and 20–29. It was found that 20–29 fragment formed exclusively flat-ribbons, which were around 40 nm in width. However, 8–37 fragment, similar to the full-length amylin, formed fibril polymorphs with variable morphologies. Most of them were left-handed cables with 25 or 50 nm cross-over and flat-like ribbons [32]. Thus, based on this observation, authors proposed that peptide sequence was directly responsible for the determination of the fibril morphology.

2.5.1. Changes in supramolecular chirality upon fibril disintegration

Recently, Kurouski et al. explored how supramolecular architecture of insulin fibrils could be changed by bacterial chaperonins. The interactions of heat shock proteins with amyloid fibrils have drawn significant attention in recently years. However, most of these studies focused on one group of heat shock proteins with small molecular mass, so called small heat shock proteins [65–67]. Many small heat shock proteins have been reported to disassemble fibrils or prevent the fibrillation process *in vitro* [68].

Kurouski et al. investigated the effect on the mutant chaperonin complex from *Pyrococcusfuriosus* (Pf) on insulin fibrils [69]. This chaperonin (Cpn) was composed of identical subunits and commonly found in most hyperthermophiles [70]. Cpn was mutated to reach its optimum activity below 50°C. Using AFM, Kurouski et al. found that after 5 min of incubation of insulin fibrils with Cpn, fibrils were found fragmented (**Figure 11**) [69].

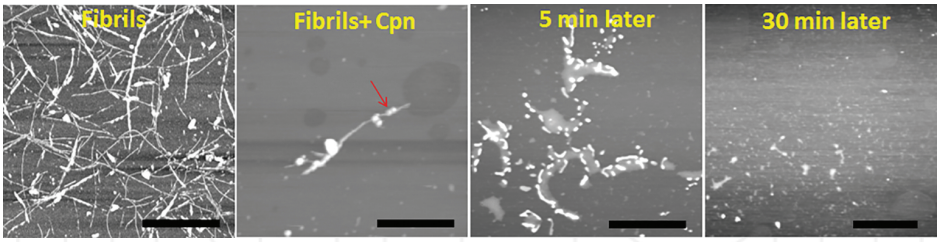

Figure 11. AFM kinetic examination of the insulin fibrils (Fibrils) mixed with Cpn and deposited right away (Fibrils + Cpn), five (5 min later) and half an hour (30 min later) later on mica surface. Immediately upon mixing, Cpn absorb on the fibril surfaces (shown with red arrow). As a result of these Cpn-Fibril interactions the last swell and break apart (5 min later). Even some fibril fragments that are evident on the early microscopic examination (5 min later) disappear after 30 min (30 min later). The scale bar is 1 μm [69].

The foreshortened fibrils looked like swollen clamps with significantly lower height (~6 nm) and width up to 200–400 nm. Interestingly, white image features on the edges of these clamps mimicked the outline of the original fibrils. Most likely they were fibrillar regions that were not melted by Cpn because the reaction was quickly terminated. These observations confirmed that Cpn was able to change the fibril architecture. Kurouski et al. concluded that Cpn melted the fibril core and formed an amorphous protein mass from regular β-sheet structure. Microscopic observations of this phenomenon also indicated a fibril swelling. Authors also found that longer exposure of insulin fibrils to Cpn resulted in their further fragmentation into smaller and smaller species with irregular shapes. These species coagulated during late stages, forming large amorphous aggregates. Most of the fibril-shaped species disappeared and predominantly amorphous objects form after 30 min of Cpn-fibril co-incubation were observed (**Figure 11**) [69].

In this section, supramolecular organization of amyloid fibrils that were formed by most of known amyloid-associated proteins was discussed. It was shown that an aggregation of these proteins may result in either flat, left- or right-twisted fibrils. Very often several different fibril polymorphs can be grown simultaneously. Numerous research findings indicate that fibril polymorphism can be controlled by pH. At the same time, there are several studies which showed that amino acid sequence can determine supramolecular organization of amyloid fibrils. This section also demonstrated that microscopy can be utilized to monitor changes in the fibril morphology during fibril formation. Moreover, microscopy can be used to monitor changes in the structure of mature fibrils, which can be initiated by chemical or physical factors, or triggered by biological molecules, such as chaperonins. Based on these finding one can envision that amyloid fibrils are dynamic rather than static thermodynamic systems and that

small change in pH or salinity may change fibril morphology or aggregation state of fibrils at the interfaces.

3. Vibrational circular dichroism a unique tool for the determination of fibril supramolecular organization

VCD is a unique spectroscopic technique that is capable of probing supramolecular chirality of amyloid fibrils [19, 42, 71]. In VCD, left (L)- and right (R)-circularly polarized infra-red (IR) light pass through the sample. It is well known that solutions of two enantiomers have different absorption of left- vs right-circularly polarized light. This physical principle is used to determine the absolute configuration or small chiral molecules, as well as to unravel supramolecular organization of macromolecules. VCD probes deeper levels of fibril supramolecular chiral organization that may not be apparent to existing forms of microscopy [8]. It was also shown that enhanced VCD sensitivity arose directly from the long-range supramolecular chirality of fibril structures at all hierarchical levels [11]. Measey and Schweitzer-Stenner modeled VCD spectra of a fibril filament that had only two peptide units long, run perpendicular to the filament axis direction [72]. The model was based on exciton coupling among amide I transition dipoles arrayed as dual, stacked β-sheet ribbons. They introduced a 2° left-hand twist between the strands yielding a long-range gradual helical twist of the filament with a one full-turn distance of 180 strands. It was found that such a structure yields enhanced VCD with a negative VCD band near 1620 cm^{-1} and a positive VCD band to higher wavenumber frequencies. A corresponding 2° intrastrand helical twist in the opposite direction, corresponding to a right-hand helical filament, reversed the sign of the enhanced VCD couplet and corresponds to the reversed VCD. This theoretical work demonstrated that VCD directly was capable of a determination of the supramolecular chiral organization of fibril filaments.

Recently, it has been found that insulin aggregation at pH 2.1 and higher results in the formation of fibrils that show a strong VCD spectrum with peaks near 1554, 1593, 1627, 1647, 1670 cm^{-1} that have (+ + – + +) sign pattern [42]. The fibril VCD spectrum with this sign patters was called "normal VCD." Microscopic examination of these fibrils indicated that a majority of them had a left-handed helical twist [8]. However, if the pH of the aggregation solution is lower than 2.4, the distribution of fibrils shifts to increasingly flat, tape-like, or binary fibrils as the incubation pH continues to be lowered that under microscopic examination show no noticeable chirality or twist on their surface. Nevertheless, these fibrils show a strong, but often somewhat smaller, VCD with a sign pattern (– – + – –) that is nearly the mirror-image of "normal" VCD fibril spectrum and is referred to as the "reversed" polymorph. The fact that flat tape-like fibrils show a strong reversed VCD signal indicates that they must be composed of right-handed filaments, the chirality of which lies below the limit of AFM or SEM detection. The combined VCD-microscopic studies showed that pH determines not only the net handedness of the filaments, precursors of mature fibrils, but also controls their association pathways. Left-handed filaments intertwine, forming left-handed proto-fibrils and mature fibrils that have normal VCD. On the other hand, right-handed filaments associate side-by-side, forming flat, tape-like, or binary fibrils. Thus, pH most likely alters protein-

http://dx.doi.org/10.5772/62672

solvent interactions or causes protonation of some amino acid side chains, which are lying on the surface of the filaments. These changes cause variations in the way these filaments bind together to form mature fibrils that either twist together to form braids or align side-by-side without braiding. In addition, it was discovered that pH not only determines insulin fibril morphology and net chirality at the stage of the protein aggregation, but also may dramatically change the morphology of mature fibrils and overturn their initial chirality.

Most likely, the sensitivity of amino-acid side chains to the aqueous solvent is responsible for this pH sensitivity. Moreover, different ways of constituent side-chains, exposed or not to the solvent, result in different pH sensitivity (high versus low) for the sense of filament chirality observed. This is a long-range fibril property that likely cannot be predicted, even qualitatively, without a realistic model of protein side chain influence on the sense of helical chirality as a function of pH. Moreover, the chirality of individual fibril filaments lies below the sensitivity of AFM or SEM imaging, but can be observed with VCD at the initial and subsequent stages of fibril formation [11].

A growing body of literature indicates that VCD has become a useful tool for the chiral characterization of amyloid aggregates. For example, Measey and Schweitzer-Stenner recently reported a large enhancement of VCD upon aggregation of short polypeptides [73]. They also demonstrated that mature fibrils formed from the N-terminal peptide fragment of the yeast prion protein, Sup35, and the amyloidogenic alanine-rich peptide AKY8 have opposite signed VCD. It has been also demonstrated that opposite signed VCD spectra could be obtained for mature fibrils formed from poly-L or -D glutamic acid [74]. Polyglutamic acid formed spirally twisted aggregates with handedness determined by the amino acid chirality (left-handed for Land right-handed for D).

4. Models of amyloid fibril formation

Accumulated experimental evidence suggested three protein aggregation pathways that lead to the discussed above morphological heterogeneity of amyloid fibrils. According to the first one, fibril polymorphism could be caused by deviations at the stage of monomer-monomer associations, while protein oligomers are formed [75]. Consequently, these structurally different oligomers will lead to structurally and morphologically different fibrils. For example, Srinivasan et al. recently investigated morphologies and structural organization of prefibrilar oligomers and mature fibrils formed from two murine serum amyloid A (SAA) isoforms, named SAA1.1 and SAA2.2 [75]. These two isoforms only have a difference in six amino acids [76]. SAA1.1 had an oligomer-rich fibrillation lag phase of a few days, while SAA2.2 formed small fibrils within a few hours, exhibiting virtually no lag phase [77]. Structural differences of SAA 1.1 and SAA 2.2 resulted in morphological differences of their filaments and consequently fibrils. Specifically, SAA 2.2 formed worm-like filaments that were able to coil and braid. At the same time, the filaments and proto-fibrils of SAA 1.1 had a rod-like supramolecular organization. They were unable to braid and formed thick straight fibrils. Using CD and Raman spectroscopy Srinivasan et al. confirmed structural differences between SAA 1.1 and SAA 2.2 oligomers and fibrils.

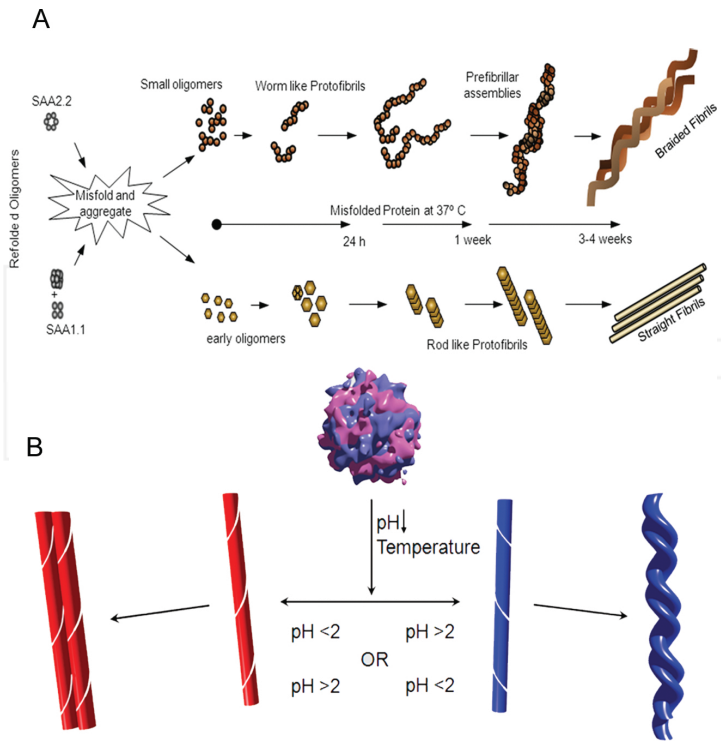

Scheme 1. Models of amyloid fibril formation. Differences in the morphology of mature fibrils can be caused by different ways of protein-protein aggregation on the stage of fibril oligomers' formation (A). Alternatively, protein aggregation leads to the formation of a filament that is able to intertwine forming twisted fibrils, or associate side-by-side (B). In the late case, tape-like fibrils are formed. Adapted from Srinivasan et al. [77] and Kurouski et al. [11].

Alternatively, the heterogeneity of fibril morphologies could be due to different ways of filament associations. Specifically, fibril filaments can either braid and coil or associate side-by-side, forming twisted or tape-like fibrils, respectively (**Scheme 1B**). These morphologically different fibrils will consequently have the same structure [8, 11]. Recently, Kurouski et al. investigated polymorphism of insulin, lysozyme, apo-α-lactalbumin, HET-s (218–289) prion, and a short polypeptide fragment of transtherytin, TTR (105–115). Authors demonstrated that all these proteins form two distinct fibril polymorphs: tape-like and twisted. They have also found that pH directly controls which polymorph will be formed. Using IR and Raman spectroscopy it has been demonstrated that both tape-like and twisted fibril polymorphs have the same secondary structure [11].

Besides braiding and side-by-side association, filament propagation can occur via several alternative pathways. According to Jansen et al. filament fragmentation may result in short filament fragments that serve as templates for lateral rather than axial protein aggregation [62]. As a result, short fibril blocks are formed (**Scheme 2A**). These blocks tend to associate side-by-side forming the fibril that has a right-handed twist upon the microscopic examination.

http://dx.doi.org/10.5772/62672

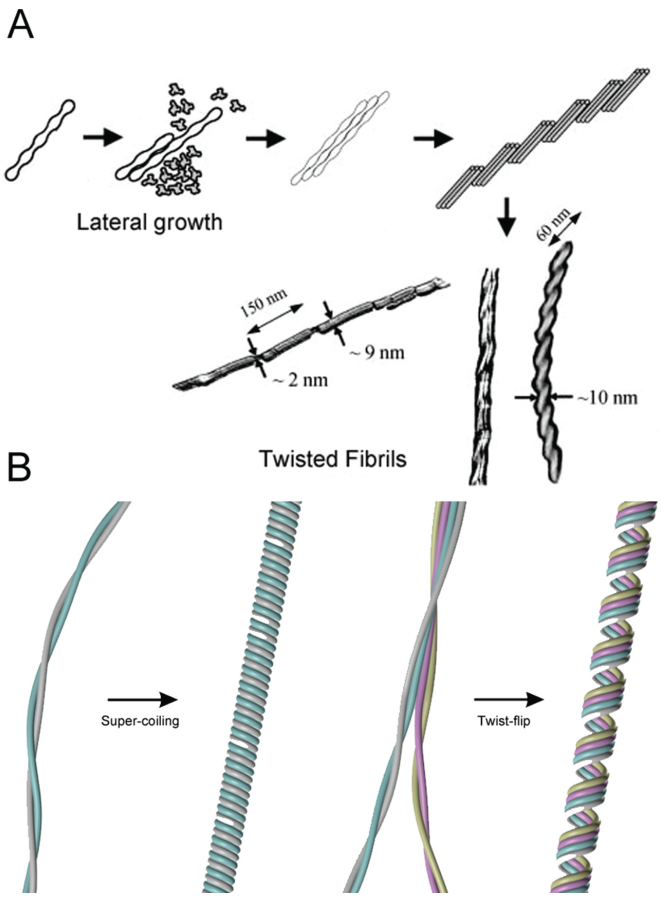

Scheme 2. Models of amyloid filament propagation. Mechanism of side-driven templation (A) and super-coiling of left-twisted fibril filament that leads to the appearance of a right-handed twist on the mature fibril (B). Adapted from R. Jansen et al. [62] and Usov et al. [53].

Separately, Usov et al. proposed two additional mechanisms that resulted in formation of morphologically different fibril polymorphs [53]. According to one, the left-twisted filament may continue twisting along the longitude axis. As a result, a hollow tube-like protein aggregate will be formed. Alternatively, it has been proposed that the left-twisted fibril filament may flip the handedness of its twist, as was discussed in the Section 2.5.

Summarizing, this chapter aimed to demonstrate how microscopy, including electron and probe microscopy, can be utilized to investigate supramolecular organization of amyloid aggregates. It demonstrated that microscopy was capable of elucidating mechanisms of fibril formation and unraveling the origin of fibril polymorphism. It was also shown that using AFM, SEM, and cryo-SEM, chiral nature of fibril supramolecular organization can be determined. The author also wanted to attract reader's attention to VCD. This powerful spectroscopic tool

is capable of probing supramolecular chirality of fibril filaments that may to always be accessible for currently available microscopic techniques.

This chapter reviewed supramolecular organization of amyloid fibrils formed by almost all known amyloidogenic proteins, including amyloid β, α-synuclein, tau, insulin, and lysozyme proteins. It demonstrated how physical and chemical factors could change morphology of fibril aggregates at the stage of their formation. It was also shown how these factors, as well as chaperonins, could change the supramolecular organization of already grown fibrils.

One should note that microscopy itself often may not be sufficient for the determination of fibril structure. Therefore, microscopy is often used with numerous spectroscopic techniques, such as ss-NMR, Raman, and IR spectroscopy. These techniques allow for the determination of ψ and φ angles of the peptide backbone, which is necessary to fully elucidate the structure of the fibril cross-β core.

Author details

Dmitry Kurouski*

Address all correspondence to: dkurouski@northwestern.edu

Chemistry Department, Northwestern University, Evanston, IL, USA

References

[1] Dobson CM. Protein folding and misfolding. Nature 2003;426:884–890.

[2] Sipe JD, Cohen AS. Review: history of the amyloid fibril. J. Struct. Biol. 2000;130:88–98.

[3] Kurouski D, Van Duyne RP, Lednev IK. Exploring the structure and formation mechanism of amyloid fibrils by Raman spectroscopy: a review. Analyst 2015;140:4967–4980.

[4] Fandrich M. On the structural definition of amyloid fibrils and other polypeptide aggregates. Cell. Mol. Life Sci. 2007;64:2066–2078.

[5] Dobson CM. Protein aggregation and its consequences for human disease. Prot. Pept. Lett. 2006;13:219–227.

[6] Usov I, Nystrom G, Adamcik J, Handschin S, Schutz C, Fall A, *et al.* Understanding nanocellulose chirality and structure-properties relationship at the single fibril level. Nat. Commun. 2015;6:7564.

[7] Assenza S, Adamcik J, Mezzenga R, De Los Rios P. Universal behavior in the mesoscale properties of amyloid fibrils. Phys. Rev. Lett. 2014;113:268103.

[8] Kurouski D, Dukor RK, Lu X, Nafie LA, Lednev IK. Normal and reversed supramolecular chirality of insulin fibrils probed by vibrational circular dichroism at the protofilament level of fibril structure. Biophys. J. 2012;103:522–531.

[9] Morozova-Roche LA, Zurdo J, Spencer A, Noppe W, Receveur V, Archer DB, et al. Amyloid fibril formation and seeding by wild-type human lysozyme and its disease-related mutational variants. J. Struct. Biol. 2000;130:339–351.

[10] Jimenez JL, Nettleton EJ, Bouchard M, Robinson CV, Dobson CM, Saibil HR. The protofilament structure of insulin amyloid fibrils. Proc. Natl. Acad. Sci. U. S. A. 2002;99:9196–9201.

[11] Kurouski D, Lu X, Popova L, Wan W, Shanmugasundaram M, Stubbs G, et al. Is supramolecular filament chirality the underlying cause of major morphology differences in amyloid fibrils? J. Am. Chem. Soc. 2014;136:2302–2312.

[12] Khurana R, Ionescu-Zanetti C, Pope M, Li J, Nielson L, Ramirez-Alvarado M, et al. A general model for amyloid fibril assembly based on morphological studies using atomic force microscopy. Biophys. J. 2003;85:1135–1144.

[13] Groenning M, Frokjaer S, Vestergaard B. Formation mechanism of insulin fibrils and structural aspects of the insulin fibrillation process. Curr. Protein Pept. Sci. 2009;10:509–528.

[14] Wischik CM, Crowther RA, Stewart M, Roth M. Subunit structure of paired helical filaments in Alzheimer's disease. J. Cell. Biol. 1985;100:1905–1912.

[15] Wischik CM, Novak M, Thogersen HC, Edwards PC, Runswick MJ, Jakes R, et al. Isolation of a fragment of tau derived from the core of the paired helical filament of Alzheimer disease. Proc. Natl. Acad. Sci. U. S. A. 1988;85:4506–4510.

[16] Kurouski D, Luo H, Sereda V, Robb FT, Lednev IK. Deconstruction of stable cross-Beta fibrillar structures into toxic and nontoxic products using a mutated archaeal chaperonin. ACS Chem. Biol. 2013;8:2095–2101.

[17] Paravastu AK, Leapman RD, Yau WM, Tycko R. Molecular structural basis for polymorphism in Alzheimer's beta-amyloid fibrils. Proc. Natl. Acad. Sci. U. S. A. 2008;105:18349–18354.

[18] Sawaya MR, Sambashivan S, Nelson R, Ivanova MI, Sievers SA, Apostol MI, et al. Atomic structures of amyloid cross-b spines reveal varied steric zippers. Nature 2007;447:453–457.

[19] Ma S, Cao X, Mak M, Sadik A, Walkner C, Freedman TB, et al. Vibrational circular dichroism shows unusual sensitivity to protein fibril formation and development in solution. J. Am. Chem. Soc. 2007;129:12364–12365.

[20] Measey TJ, Smith KB, Decatur SM, Zhao L, Yang G, Schweitzer-Stenner R. Self-aggregation of a polyalanine octamer promoted by its C-terminal tyrosine and probed

by a strongly enhanced vibrational circular dichroism signal. J. Am. Chem. Soc. 2009;131:18218–18219.

[21] Lednev LK. Amyloid fibrils: the Eighth Wonder of the world in protein folding and aggregation. Biophys. J. 2014;106:1433–1435.

[22] Betzig E, Patterson GH, Sougrat R, Lindwasser OW, Olenych S, Bonifacino JS, et al. Imaging intracellular fluorescent proteins at nanometer resolution. Science 2006;313:1642–1645.

[23] Hell SW, Wichmann J. Breaking the diffraction resolution limit by stimulated emission: stimulated-emission-depletion fluorescence microscopy. Opt. Lett. 1994;19:780–782.

[24] Heilemann M, van de Linde S, Schuttpelz M, Kasper R, Seefeldt B, Mukherjee A, et al. Subdiffraction-resolution fluorescence imaging with conventional fluorescent probes. Angew. Chem. Int. Ed. Engl. 2008;47:6172–6176.

[25] Kaminski Schierle GS, van de Linde S, Erdelyi M, Esbjorner EK, Klein T, Rees E, et al. In situ measurements of the formation and morphology of intracellular beta-amyloid fibrils by super-resolution fluorescence imaging. J. Am. Chem. Soc. 2011;133:12902–12905.

[26] Tosoni A., Barbiano di Belgiojoso G. and Nebuloni M. (2011). Electron Microscopy in the Diagnosis of Amyloidosis, Amyloidosis - Mechanisms and Prospects for Therapy, Dr. Svetlana Sarantseva (Ed.), ISBN: 978- 953-307-253-1, InTech, Available from: http://www.intechopen.com/books/amyloidosis-mechanisms-andprospects-for-therapy/electron-microscopy-in-the-diagnosis-of-amyloidosis Locatoin: University Campus STeP Ri Slavka Krautzeka 83/A 51000 Rijeka, Croatia

[27] Inoue S, Kuroiwa M, Kisilevsky R. Basement membranes, microfibrils and beta amyloid fibrillogenesis in Alzheimer's disease: high resolution ultrastructural findings. Brain Res. Rev. 1999;29:218–231.

[28] Inoue S, Kuroiwa M, Tan R, Kisilevsky R. A high resolution ultrastructural comparison of isolated and in situ murine AA amyloid fibrils. Amyloid 1998;5:99–110.

[29] Inoue S, Kuroiwa M, Saraiva MJ, Guimaraes A, Kisilevsky R. Ultrastructure of familial amyloid polyneuropathy amyloid fibrils: examination with high-resolution electron microscopy. J. Struct. Biol. 1998;124:1–12.

[30] Kidd M. Paired helical filaments in electron microscopy of Alzheimer's disease. Nature 1963;197:192–193.

[31] Goldsbury CS, Cooper GJ, Goldie KN, Muller SA, Saafi EL, Gruijters WT, et al. Polymorphic fibrillar assembly of human amylin. J. Struct. Biol. 1997;119:17–27.

[32] Goldsbury C, Goldie K, Pellaud J, Seelig J, Frey P, Muller SA, et al. Amyloid fibril formation from full-length and fragments of amylin. J. Struct. Biol. 2000;130:352–362.

[33] Shammas SL, Knowles TP, Baldwin AJ, Macphee CE, Welland ME, Dobson CM, Devlin GL. Perturbation of the stability of amyloid fibrils through alteration of electrostatic interactions. Biophys. J. 2011;100:2783–2791.

[34] Gras SL, Waddington LJ, Goldie KN. Transmission electron microscopy of amyloid fibrils. Methods Mol. Biol. 2011;752:197–214.

[35] Kurouski D, Dukor RK, Lu X, Nafie LA, Lednev IK. Spontaneous inter-conversion of insulin fibril chirality. Chem. Commun. 2012;48:2837–2839.

[36] Petkova AT, Leapman RD, Guo Z, Yau W-M, Mattson MP, Tycko R. Self-propagating, molecular-level polymorphism in Alzheimer's ÃŸ-amyloid fibrils. Science 2005;307:262–265.

[37] Sen A, Baxa U, Simon MN, Wall JS, Sabate R, Saupe SJ, Steven AC. Mass analysis by scanning transmission electron microscopy and electron diffraction validate predictions of stacked beta-solenoid model of HET-s prion fibrils. J. Biol. Chem. 2007;282:5545–5550.

[38] Wasmer C, Lange A, Van Melckebeke H, Siemer AB, Riek R, Meier BH. Amyloid fibrils of the HET-s(218–289) prion form a beta solenoid with a triangular hydrophobic core. Science 2008;319:1523–1526.

[39] Chen B, Thurber KR, Shewmaker F, Wickner RB, Tycko R. Measurement of amyloid fibril mass-per-length by tilted-beam transmission electron microscopy. Proc. Natl. Acad. Sci. U. S. A. 2009;106:14339–14344.

[40] Rubin N, Perugia E, Wolf SG, Klein E, Fridkin M, Addadi L. Relation between serum amyloid A truncated peptides and their suprastructure chirality. J. Am. Chem. Soc. 2010;132:4242–4248.

[41] Rubin N, Perugia E, Goldschmidt M, Fridkin M, Addadi L. Chirality of amyloid suprastructures. J. Am. Chem. Soc. 2008;130:4602–4603.

[42] Kurouski D, Lombardi RA, Dukor RK, Lednev IK, Nafie LA. Direct observation and pH control of reversed supramolecular chirality in insulin fibrils by vibrational circular dichroism. Chem. Commun. 2010;46:7154–7156.

[43] Meinhardt J, Sachse C, Hortschansky P, Grigorieff N, Fandrich M. Abeta(1–40) fibril polymorphism implies diverse interaction patterns in amyloid fibrils. J. Mol. Biol. 2009;386:869–877.

[44] Fandrich M, Meinhardt J, Grigorieff N. Structural polymorphism of Alzheimer Abeta and other amyloid fibrils. Prion 2009;3:89–93.

[45] Antzutkin ON. Amyloidosis of Alzheimer's Abeta peptides: solid-state nuclear magnetic resonance, electron paramagnetic resonance, transmission electron microscopy, scanning transmission electron microscopy and atomic force microscopy studies. Magn. Reson. Chem. 2004;42:231–246.

[46] Klement K, Wieligmann K, Meinhardt J, Hortschansky P, Richter W, Fandrich M. Effect of different salt ions on the propensity of aggregation and on the structure of Alzheimer's abeta(1–40) amyloid fibrils. J. Mol. Biol. 2007;373:1321–1333.

[47] Petkova AT, Leapman RD, Guo Z, Yau WM, Mattson MP, Tycko R. Self-propagating, molecular-level polymorphism in Alzheimer's beta-amyloid fibrils. Science 2005;307:262–265.

[48] Luhrs T, Ritter C, Adrian M, Riek-Loher D, Bohrmann B, Dobeli H, et al. 3D structure of Alzheimer's amyloid-beta(1–42) fibrils. Proc. Natl. Acad. Sci. U. S. A. 2005,102:17342–17347.

[49] Zhang R, Hu X, Khant H, Ludtke SJ, Chiu W, Schmid MF, et al. Interprotofilament interactions between Alzheimer's Abeta1–42 peptides in amyloid fibrils revealed by cryoEM. Proc. Natl. Acad. Sci. U. S. A. 2009;106:4653–4658.

[50] Vilar M, Chou HT, Luhrs T, Maji SK, Riek-Loher D, Verel R, et al. The fold of alpha-synuclein fibrils. Proc. Natl. Acad. Sci. U. S. A. 2008;105:8637–8642.

[51] Crowther RA, Daniel SE, Goedert M. Characterisation of isolated alpha-synuclein filaments from substantia nigra of Parkinson's disease brain. Neurosci. Lett. 2000;292:128–130.

[52] Spillantini MG, Crowther RA, Jakes R, Cairns NJ, Lantos PL, Goedert M. Filamentous alpha-synuclein inclusions link multiple system atrophy with Parkinson's disease and dementia with Lewy bodies. Neurosci. Lett. 1998;251:205–208.

[53] Usov I, Adamcik J, Mezzenga R. Polymorphism complexity and handedness inversion in serum albumin amyloid fibrils. ACS Nano 2013;7:10465–10474.

[54] Adamcik J, Mezzenga R. Adjustable twisting periodic pitch of amyloid fibrils. Soft Matter 2011;7:5437–5443.

[55] Jordens S, Isa L, Usov I, Mezzenga R. Non-equilibrium nature of two-dimensional isotropic and nematic coexistence in amyloid fibrils at liquid interfaces. Nat. Commun. 2013;4:1917.

[56] Jordens S, Ruhs PA, Sieber C, Isa L, Fischer P, Mezzenga R. Bridging the gap between the nanostructural organization and macroscopic interfacial rheology of amyloid fibrils at liquid interfaces. Langmuir 2014;30:10090–10097.

[57] Loksztejn A, Dzwolak W. Chiral bifurcation in aggregating insulin: an induced circular dichroism study. J. Mol. Biol. 2008;379:9–16.

[58] Dzwolak W, Pecul M. Chiral bias of amyloid fibrils revealed by the twisted conformation of Thioflavin T: an induced circular dichroism/DFT study. FEBS Lett. 2005,579:6601–6603.

[59] Dzwolak W. Vortex-induced chiral bifurcation in aggregating insulin. Chirality 2010;22(Suppl. 1):E154–E160.

[60] Campioni S, Carret G, Jordens S, Nicoud L, Mezzenga R, Riek R. The presence of an air-water interface affects formation and elongation of alpha-Synuclein fibrils. J. Am. Chem. Soc. 2014;136:2866–2875.

[61] Qin Z, Hu D, Han S, Hong DP, Fink AL. Role of different regions of alpha-synuclein in the assembly of fibrils. Biochemistry 2007;46:13322–13330.

[62] Jansen R, Dzwolak W, Winter R. Amyloidogenic self-assembly of insulin aggregates probed by high resolution atomic force microscopy. Biophys. J. 2005;88:1344–1353.

[63] Goldsbury C, Kistler J, Aebi U, Arvinte T, Cooper GJ. Watching amyloid fibrils grow by time-lapse atomic force microscopy. J. Mol. Biol. 1999;285:33–39.

[64] Goldsbury C, Baxa U, Simon MN, Steven AC, Engel A, Wall JS, et al. Amyloid structure and assembly: insights from scanning transmission electron microscopy. J. Struct. Biol. 2010;173:1–13.

[65] Lee S, Carson K, Rice-Ficht A, Good T. Small heat shock proteins differentially affect Abeta aggregation and toxicity. Biochem. Biophys. Res. Commun. 2006;347:527–533.

[66] Wilhelmus MM, Boelens WC, Otte-Holler I, Kamps B, de Waal RM, Verbeek MM. Small heat shock proteins inhibit amyloid-beta protein aggregation and cerebrovascular amyloid-beta protein toxicity. Brain. Res. 2006;1089:67–78.

[67] Raman B, Ban T, Sakai M, Pasta SY, Ramakrishna T, Naiki H, et al. AlphaB-crystallin, a small heat-shock protein, prevents the amyloid fibril growth of an amyloid beta-peptide and beta2-microglobulin. Biochem. J. 2005;392:573–581.

[68] Ecroyd H, Carver JA. Crystallin proteins and amyloid fibrils. Cell. Mol. Life Sci. 2009;66:62–81.

[69] Kurouski D, Luo H, Sereda V, Robb FT, Lednev IK. Rapid degradation kinetics of amyloid fibrils under mild conditions by an archaeal chaperonin. Biochem. Biophys. Res. Commun. 2012;422:97–102.

[70] Laksanalamai P, Robb FT. Small heat shock proteins from extremophiles: a review. Extremophiles 2004;8:1–11.

[71] Nafie LA. Vibrational Optical Activity: Principles and Applications. Chichester: Wiley; 2011. 398 p.

[72] Measey TJ, Schweitzer-Stenner R. Vibrational circular dichroism as a probe of fibrillogenesis: the origin of the anomalous intensity enhancement of amyloid-like fibrils. J. Am. Chem. Soc. 2010;133:1066–1076.

[73] Fulara A, Lakhani A, Wojcik S, Nieznanska H, Keiderling TA, Dzwolak W. Spiral superstructures of amyloid-like fibrils of polyglutamic acid: an infrared absorption and vibrational circular dichroism study. J. Phys. Chem. B 2011;115:11010–11016.

[74] Yu J, Zhu H, Guo JT, de Beer FC, Kindy MS. Expression of mouse apolipoprotein SAA1.1 in CE/J mice: isoform-specific effects on amyloidogenesis. Lab. Invest. 2000;80:1797–1806.

[75] Malle E, Sodin-Semrl S, Kovacevic A. Serum amyloid A: an acute-phase protein involved in tumour pathogenesis. Cell. Mol. Life Sci. 2009;66:9–26.

[76] Srinivasan S, Patke S, Wang Y, Ye Z, Litt J, Srivastava SK, et al. Pathogenic serum amyloid A 1.1 shows a long oligomer-rich fibrillation lag phase contrary to the highly amyloidogenic non-pathogenic SAA2.2. J. Biol. Chem. 2013;288:2744–2755.

[77] Kurouski D, Handen JD, Dukor RK, Nafie LA, Lednev IK. Supramolecular chirality in peptide microcrystals. Chem. Commun. 2015;51:89–92.